Nanoscale

COMMUNICATION

View Article Online
View Journal | View Issue

Cite this: *Nanoscale*, 2019, **11**, 4226

Received 14th January 2019,
Accepted 13th February 2019

DOI: 10.1039/c9nr00412b

rsc.li/nanoscale

Sub-10 nm stable graphene quantum dots embedded in hexagonal boron nitride†

Dongxue Chen,‡[a,b,c] Ruixi Qiao,‡[b] Xiaozhi Xu,[b] Weikang Dong,[d] Li Wang,[b,e] Ruisong Ma,[e] Can Liu,[b] Zhihong Zhang,[b] Muhong Wu,[b] Lei Liu,[f] Lihong Bao,[e] Hui-Tian Wang,[c] Peng Gao,[d] Kaihui Liu*[b] and Dapeng Yu*[a,g]

Graphene quantum dots (GQDs), a zero-dimensional material system with distinct physical properties, have great potential in the applications of photonics, electronics, photovoltaics, and quantum information. In particular, GQDs are promising candidates for quantum computing. In principle, a sub-10 nm size is required for GQDs to present the intrinsic quantum properties. However, with such an extreme size, GQDs have predominant edges with lots of active dangling bonds and thus are not stable. Satisfying the demands of both quantum size and stability is therefore of great challenge in the design of GQDs. Herein we demonstrate the fabrication of sub-10 nm stable GQD arrays by embedding GQDs into large-bandgap hexagonal boron nitride (h-BN). With this method, the dangling bonds of GQDs were passivated by the surrounding h-BN lattice to ensure high stability, meanwhile maintaining their intrinsic quantum properties. The sub-10 nm nanopore array was first milled in h-BN using an advanced high-resolution helium ion microscope and then GQDs were directly grown in them through the chemical vapour deposition process. Stability analysis proved that the embedded GQDs show negligible property decay after baking at 100 °C in air for 100 days. The success in preparing sub-10 nm stable GQD arrays will promote the physical exploration and potential applications of this unique zero-dimensional in-plane quantum material.

Introduction

Among broad low-dimensional materials,[1–3] zero-dimensional quantum dots are an important family member and present rich quantum properties and wide applications.[4,5] As an emerging in-plane zero-dimensional material originating from the star material of two-dimensional graphene, graphene quantum dots (GQDs) exhibit rich properties superior to conventional semiconductor quantum dots.[6–22] Theoretical calculations reveal that a large tunable bandgap from 0 eV of infinite graphene sheets to ~7 eV of benzene can be accurately engineered for GQDs by varying their size and morphology.[7,8] Weak spin–orbit coupling and the absence of hyperfine interactions of carbon-based materials provide GQDs possibilities for spin qubits with long coherence times up to 100 ns.[9] GQDs have also been reported to show low cytotoxicity, excellent biocompatibility and environmental friendliness in contrast to conventional semiconductor quantum dots made from toxic heavy metals.[10] All of these intriguing properties make GQDs a promising material for optoelectronics,[11] photonics,[12,13] biomedicine,[14,15] electronics,[16–20] and quantum computation.[21,22] In principle, to exhibit the intrinsic quantum properties of GQDs, their size must shrink into the range of typically sub-10 nm to ensure strong quantum confinement.[6,10] However, once the size reaches the sub-10 nm scale, the predominant edges with lots of active dangling bonds make GQDs unstable.[23–26] It seems that the quantum size and stability of GQDs are incompatible with each other.

In the past 10 years, great efforts have been made to fabricate sub-10 nm-scale stable GQDs. One prevailing strategy is to decompose or exfoliate bulk graphite into graphene flakes by chemical or physical routes such as hydrothermal cutting, electrochemical cutting, and microwave-assisted or ultrasonic shearing.[27–31] However, in these methods, the GQDs have a broad size distribution and lots of chemical species reconstructed and adsorbed on the dangling bonds of the GQD edges, which prevent the presence of their intrinsic quantum properties. Another strategy is based on high-resolution

[a]*Institute for Quantum Science and Engineering and Department of Physics, Southern University of Science and Technology, Shenzhen 518055, China. E-mail: yudp@sustc.edu.cn*
[b]*State Key Laboratory for Mesoscopic Physics, Collaborative Innovation Center of Quantum Matter, School of Physics, Peking University, Beijing 100871, China. E-mail: khliu@pku.edu.cn*
[c]*School of Physics, Nankai University, Tianjin 300071, China*
[d]*Electron Microscopy Laboratory, School of Physics, Peking University, Beijing 100871, China*
[e]*Institute of Physics, Chinese Academy of Sciences, Beijing 100190, China*
[f]*Department of Materials Science and Engineering, College of Engineering, Peking University, Beijing 100871, China*
[g]*Shenzhen Key Laboratory of Quantum Science and Engineering, Shenzhen 518055, China*

†Electronic supplementary information (ESI) available: Measurement of EELS and STEM characterization. See DOI: 10.1039/c9nr00412b

‡These authors contributed equally to this research work.

lithography on graphene films. With this technique, one can precisely cut graphene to a designed size and shape, thus producing uniform GQDs.[32] But the size obtained is typically above tens of nanometres (due to the resolution limit in conventional lithography fabrication), and the GQD edges are unstable. The chemical vapour deposition (CVD) method was also applied to grow GQDs directly, but the obtained size was still in the order of 100 nm to microns.[33] Therefore, finding ways to fabricate GQDs with both quantum size and high stability is still a great challenge until now.

Here for the first time, we demonstrate the fabrication of sub-10 nm GQD arrays with high stability of more than 100 days at 100 °C. The starting point of our design is to embed GQDs into a lattice-matching material to passivate the dangling bonds of GQDs to ensure stabilization. Meanwhile, this material should be a large-bandgap insulator to maintain the intrinsic properties of GQDs. Hexagonal boron nitride (h-BN), a high-profile 2D insulating material with a wide bandgap of ~6 eV, is chosen for this purpose as it has the similar crystal symmetry and lattice constant to graphene (only 1.7% mismatch).[33–36] We utilized the high-resolution fabrication ability of a helium ion microscope (HIM) to directly mill a sub-10 nm nanopore array on h-BN followed by the CVD method to grow GQDs inside these nanopores. The successful fabrication of the sub-10 nm stable GQD array will promote their practical applications and physical exploration in this zero-dimensional in-plane quantum material.

Results and discussion

In our experiment, h-BN flakes were first capped onto Cu foil by mechanical exfoliation method. Then nanopore arrays were directly milled on these flakes using an advanced focus helium ion microscope with sub-nanometre resolution (Fig. 1a). Compared with the traditional gallium ion beam microscope, in the helium ion microscope helium has a much smaller mass and therefore gives much better spatial resolution.[37,38] Afterwards, the GQDs were synthesized into these nanopores to form the GQD-BN embedded structure (Fig. 1b) by low pressure chemical vapour deposition (see the Experimental section for more details of the growth process). Finally, the synthesized GQDs were transferred onto SiO_2/Si or other target substrates for further characterization (Fig. 1c). With this technique, one can accurately fabricate nanopore arrays with designed size (as small as 4 nm) and patterns (Fig. 1d–f).

To check the quality of as-grown GQDs, Raman spectroscopy was first conducted after the material was transferred onto the SiO_2/Si substrate. For the area without h-BN flakes, the characteristic G mode and 2D mode of graphene can be observed (olive curve shown in Fig. 2a). The 2D/G intensity ratio of ~2 and the weak D mode demonstrate that high-quality monolayer graphene is synthesized on the Cu surface without h-BN flakes. The Raman spectrum on bare h-BN only shows the E_{2g} mode of h-BN at 1374 cm^{-1} without any detectable signal of graphene (orange curve shown in Fig. 2a), revealing the absence of epitaxial graphene growth above or below h-BN under our growth conditions. In contrast, as for the Raman spectrum on the GQD region (dark yellow curve shown in Fig. 2a), the E_{2g} mode of h-BN as well as the G and 2D modes of graphene co-exist, revealing that graphene is indeed grown in the nanopores of h-BN (the laser spot size is larger than the GQD size). The appearance of D and D′ modes should be attributed to the edges of GQDs.[39,40]

To further confirm the embedded GQD-BN structure, the as-grown sample was transferred onto holey carbon film transmission electron microscope (TEM) grids (Fig. 2b) and charac-

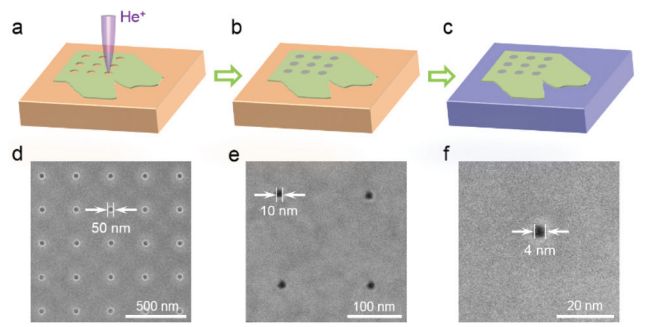

Fig. 1 Schematic diagrams of (a) helium ion microscope-based fabrication of a nanopore array on h-BN, (b) synthesis of a GQD array embedded in h-BN, (c) a GQD array embedded in h-BN transferred to another substrate, and (d–f) nanopores on h-BN with diameters of 50 nm, 10 nm and 4 nm, respectively.

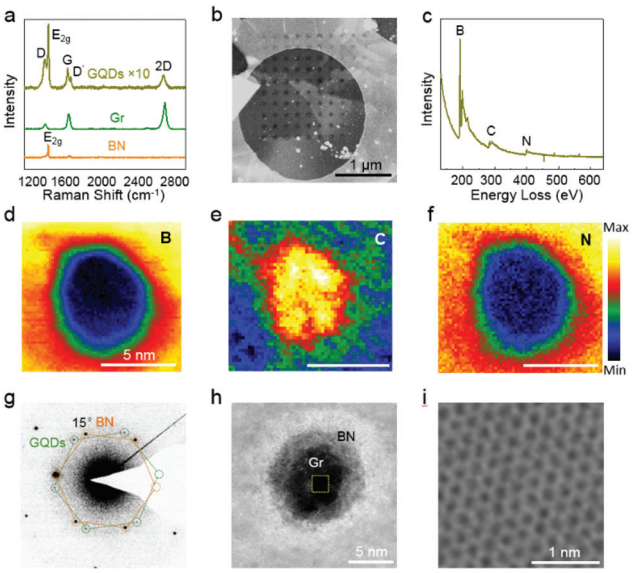

Fig. 2 (a) Raman spectra of h-BN (orange), graphene (olive) and the GQD array embedded in a h-BN flake (dark yellow), respectively. (b) Low magnification STEM image of the GQD array in h-BN nanopores. The circle in this figure is a hollow carbon film of TEM grids. (c) EELS spectrum of the GQD array embedded in h-BN. (d–f) Corresponding EELS mapping of boron, carbon and nitrogen (c) in STEM mode. (g) SAED pattern of a GQD embedded in h-BN. (e) STEM image of GQDs and h-BN heterojunction. (h) An atomically resolved image of the GQDs in the area marked by a yellow box is shown in (i).

terized by electron energy loss spectroscopy (EELS). The detected peaks (Fig. 2c; ESI Fig. S1†) verify the chemical components of boron, carbon and nitrogen.[41–43] Further EELS mapping of boron (Fig. 2d), carbon (Fig. 2e) and nitrogen (Fig. 2f) in scanning transmission electron microscopy (STEM) mode provides unambiguous evidence for the existence of GQDs inside h-BN. Then we carried out selected-area electron diffraction (SAED) and STEM to investigate the structural information of the GQD array in both the reciprocal space and real space. The diffraction pattern shows two sets of hexagonal diffraction patterns with an ~15° twist angle (Fig. 2g), corresponding to graphene and h-BN lattice (the electron beam area is larger than the GQD size).[34] The STEM images of graphene show atomically resolved carbon hexagons (Fig. 2h–i; ESI Fig. S2†), demonstrating that GQDs have been successfully embedded in the nanopores of h-BN.

By milling nanopores on exfoliated h-BN, we successfully realized the fabrication of GQDs with sub-10 nm size. However, these exfoliated h-BN flakes are of small size and cannot meet the demand of large-scale applications. Thus, pushing this method to large-scale h-BN films is very significant for further real applications. To verify the universality of our method, the CVD grown h-BN monolayer was used[44] and nanopores with a typical size of ~4 nm were milled by the same procedure as that on exfoliated h-BN flakes (Fig. 3a and b). Raman spectroscopy showed that GQDs were also synthesized in the nanopores of the CVD-grown h-BN monolayer (Fig. 3c). The GQD array was transferred onto holey carbon film TEM grids supported by a monolayer graphene film and characterized by TEM (the CVD-grown h-BN monolayer is fragile if there is no support of the graphene film). The SEAD pattern shows the signal of both GQDs and the graphene film in Fig. 3d and e (the electron beam area is smaller than the GQD size here). The high-resolution transmission electron microscopy (HRTEM) image shows the Moiré pattern of GQDs and the graphene film (Fig. 3f) and the period of ~1.17 nm is consistent with the twist angle of ~12° as in the SAED pattern. This characterization demonstrates unambiguously that GQDs are embedded in the nanopores of the CVD-grown h-BN monolayer.

As the edges and dangling bonds are passivated by surrounding h-BN lattice, the stability of as-grown GQDs should be greatly improved. To verify this expectation, a comparative experiment of stability between commercially available GQDs (~5 nm in diameter) and our embedded GQDs was conducted. For the commercial GQDs, the signal of Raman spectrum is too weak to detect even after heating in air at 100 °C for only 5 min (Fig. 4a). Meanwhile, it is much easier to distinguish the variation by photoluminescence (PL) signal. The intensity of the PL peak declined sharply within a few minutes after heating in air at 100 °C (Fig. 4b). In just 5 minutes, the intensity dropped to one-tenth of its original level and became undetectable in 60 minutes. At a lower temperature of 90 °C or 80 °C, the continuously tracked PL intensity shows an obvious decrease as well (Fig. 4c), suggesting the instability of conventionally isolated GQDs. Here we note that the intrinsic bandgap of GQDs with a diameter of 5 nm should be around 0.2 eV (6200 nm in the PL spectrum) from equation ΔE (eV) ≈ $1/D$ (nm),[45,46] where D is the diameter of the GQD, and the observed PL in commercial GQDs in the visible range is a signature for the presence of extrinsic quantum effects likely due to the unsaturated edges adsorbed with nitrides and sulphides (ESI Fig. S3†). This observation is consistent with previous reports that the ordinary GQDs will have extrinsic quantum effects due to the adsorption of chemical species or functional groups.[47–49] Instead, our GQDs show a clear Raman feature of graphitic materials but no PL in the visible range (Fig. 4d),

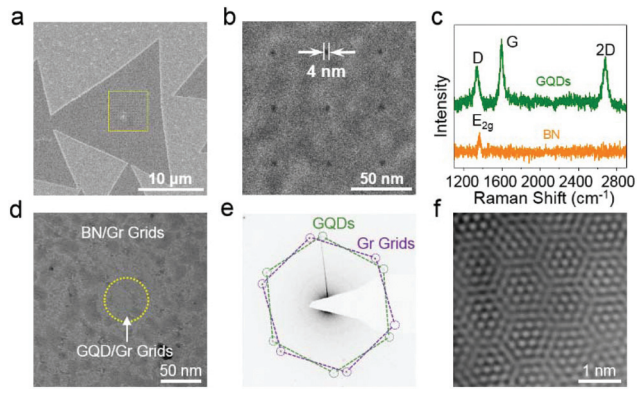

Fig. 3 (a) Helium ion microscopy image of the nanopore array milled on the CVD-grown h-BN monolayer. (b) Helium ion microscopy image of the nanopore array with a diameter of 4 nm. (c) Raman spectra of h-BN (orange) and the GQD array embedded in h-BN (olive). (d) A low-magnification TEM image of GQDs (yellow dotted circle) embedded in CVD-grown h-BN as supported by a graphene TEM film. (e) SAED pattern of GQDs shown in (d). (f) HRTEM image of the Moiré pattern of GQDs and the graphene TEM film shown in (d).

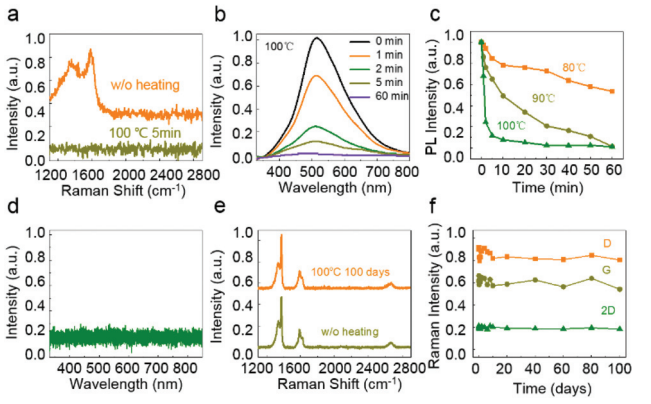

Fig. 4 (a) Raman spectrum of commercial GQDs. (b) Photoluminescence spectra of commercial GQDs baked in air with different times at 100 °C. (c) The intensity evolution of the photoluminescence spectra of commercial GQDs baked at different temperatures. (d) Photoluminescence spectrum of GQDs embedded in h-BN. (e) Raman spectra of GQDs embedded in h-BN baked at 100 °C before (dark yellow) and after 100 days (orange). (f) The intensity evolution of D, G and 2D modes of GQDs during baking in air at 100 °C with different times.

while for our GQDs embedded in h-BN, the Raman spectra remained almost invariable even after heating in air at 100 °C for 100 days (Fig. 4e and f), revealing the great stability of our GQD materials.

Conclusions

The success in preparing the sub-10 nm stable GQD array in both exfoliated h-BN flakes and CVD-grown h-BN monolayers will promote the large-scale applications of GQDs. For example, with lower atomic weights of GQDs, the coherence times of spin qubits could increase due to weak spin–orbit coupling and the absence of hyperfine interactions of carbon, which makes GQDs a promising candidate for quantum computation. In addition, the embedding technique combined with high-resolution fabrication with the helium ion microscope may pave new directions for other air-stable quantum materials from broad two-dimensional materials, such as transition metal dichalcogenides, silicene, stanene, germanene, phosphorene and so on, and therefore establish a broad materials system of zero-dimensional in-plane quantum dots with a sub-10 nm size and good stability.

Experimental

GQD growth

GQDs were grown in a tube furnace (Hefei Kejing Co. Ltd) by CVD at a pressure of about 200 Pa. The CVD system was gradually heated up to 1000 °C for exfoliated h-BN or 850–1000 °C for CVD-synthesized h-BN under 50 sccm Ar and 2 sccm H_2. 10 sccm of CH_4 was introduced during the growth of GQDs for 5 min. After growth, the CVD system was cooled down to room temperature quickly under the protection of mixed Ar and H2 flow.

h-BN preparation

Mechanically exfoliated h-BN was directly capped onto copper (25 μm thick, 99.8%, Sichuan Oriental Stars Trading Co. Ltd). CVD-synthesized h-BN was grown on the same type of copper with ammonia borane (NH_3–BH_3) as a precursor. The CVD system was heated to 1000 °C at atmospheric pressure under 500 sccm Ar and 5 sccm H_2. The precursor ammonia borane was heated to 75 °C using a heating belt and sublimated during the growth. After growth, the CVD system was cooled down to room temperature under the protection of mixed Ar and H_2 flow.

Transfer

The GQDs synthesized in mechanically exfoliated h-BN were transferred onto SiO_2/Si or commercial holey carbon film TEM grids (Zhongjingkeyi GIG-2010-3C) by a regular approach using polymethyl methacrylate (PMMA). The GQDs synthesized in CVD-grown h-BN were transferred onto homemade monolayer graphene TEM grids, which is achieved by transferring large-area monolayer single-crystal graphene on commercial TEM grids mentioned above in advance.

Fabrication & characterization methods

Milling of the nanopore array in h-BN was performed using a Zeiss Orion NanoFab. Raman spectra were recorded using a HORIBA LabRAM HR800 with a 633 nm laser. Photoluminescence spectra were recorded using a HORIBA LabRAM HR Evolution with a 325 nm laser. HRTEM, STEM, SAED and EELS experiments were performed in an aberration-corrected FEI Titan Themis G2 300 operating at an accelerating voltage of 80 kV.

Conflicts of interest

The authors declare no conflict of interest.

Acknowledgements

This work was supported by the National Key R&D Program of China (2016YFA0300804 and 2016YFA0300903), Science, Technology and Innovation Commission of Shenzhen Municipality (ZDSYS20170303165926217 and JCYJ20170412152620376), Guangdong Innovative and Entrepreneurial Research Team Program (2016ZT06D348), NSFC (51522201, 11474006 and 51672007), National Equipment Program of China (ZDYZ2015-1), Beijing Graphene Innovation Program (Z161100002116028), National Postdoctoral Program for Innovative Talents (BX201700014) and China Postdoctoral Science Foundation (2017M611148 and 2018M630017).

References

1 M. Chhowalla, H. S. Shin, G. Eda, L. J. Li, K. P. Loh and H. Zhang, *Nat. Chem.*, 2013, **5**, 263–275.
2 K. S. Novoselov, A. Mishchenko, A. Carvalho and A. H. C. Neto, *Science*, 2016, **353**, 6298.
3 H. Zhang, H. M. Cheng and P. D. Ye, *Chem. Soc. Rev.*, 2018, **47**, 6009–6012.
4 S. De Franceschi, L. Kouwenhoven, C. Schonenberger and W. Wernsdorfer, *Nat. Nanotechnol.*, 2010, **5**, 703–711.
5 X. Z. Lan, S. Masala and E. H. Sargent, *Nat. Mater.*, 2014, **13**, 233–240.
6 Z. P. Zhang, J. Zhang, N. Chen and L. T. Qu, *Energy Environ. Sci.*, 2012, **5**, 8869–8890.
7 G. Eda, Y. Y. Lin, C. Mattevi, H. Yamaguchi, H. A. Chen, I. S. Chen, C. W. Chen and M. Chhowalla, *Adv. Mater.*, 2010, **22**, 505–509.
8 X. Z. Xu, C. Liu, Z. H. Sun, T. Cao, Z. H. Zhang, E. G. Wang, Z. F. Liu and K. H. Liu, *Chem. Soc. Rev.*, 2018, **47**, 3059–3099.
9 C. Volk, C. Neumann, S. Kazarski, S. Fringes, S. Engels, F. Haupt, A. Muller and C. Stampfer, *Nat. Commun.*, 2013, **4**, 1753.

10 X. M. Li, M. C. Rui, J. Z. Song, Z. H. Shen and H. B. Zeng, *Adv. Funct. Mater.*, 2015, **25**, 4929–4947.
11 V. Gupta, N. Chaudhary, R. Srivastava, G. D. Sharma, R. Bhardwaj and S. Chand, *J. Am. Chem. Soc.*, 2011, **133**, 9960–9963.
12 D. I. Son, B. W. Kwon, D. H. Park, W. S. Seo, Y. Yi, B. Angadi, C. L. Lee and W. K. Choi, *Nat. Nanotechnol.*, 2012, **7**, 465–471.
13 D. Y. Pan, J. C. Zhang, Z. Li and M. H. Wu, *Adv. Mater.*, 2010, **22**, 734–738.
14 J. C. Ge, M. H. Lan, B. J. Zhou, W. M. Liu, L. Guo, H. Wang, Q. Y. Jia, G. L. Niu, X. Huang, H. Y. Zhou, X. M. Meng, P. F. Wang, C. S. Lee, W. J. Zhang and X. D. Han, *Nat. Commun.*, 2014, **5**, 4596.
15 D. Kim, J. M. Yoo, H. Hwang, J. Lee, S. H. Lee, S. P. Yun, M. J. Park, M. Lee, S. Choi, S. H. Kwon, S. Lee, S. H. Kwon, S. Kim, Y. J. Park, M. Kinoshita, Y. H. Lee, S. Shin, S. R. Paik, S. J. Lee, S. Lee, B. H. Hong and H. S. Ko, *Nat. Nanotechnol.*, 2018, **13**, 812–818.
16 T. Dirks, T. L. Hughes, S. Lal, B. Uchoa, Y. F. Chen, C. Chialvo, P. M. Goldbart and N. Mason, *Nat. Phys.*, 2011, **7**, 386–390.
17 M. R. Connolly, K. L. Chiu, S. P. Giblin, M. Kataoka, J. D. Fletcher, C. Chua, J. P. Griffiths, G. A. C. Jones, V. I. Falko, C. G. Smith and T. J. B. M. Janssen, *Nat. Nanotechnol.*, 2013, **8**, 417–420.
18 C. Gutierrez, L. Brown, C. J. Kim, J. Park and A. N. Pasupathy, *Nat. Phys.*, 2016, **12**, 1069–1075.
19 A. El Fatimy, R. L. Myers-Ward, A. K. Boyd, K. M. Daniels, D. K. Gaskill and P. Barbara, *Nat. Nanotechnol.*, 2016, **11**, 335–338.
20 N. M. Freitag, T. Reisch, L. A. Chizhova, P. Nemes-Incze, C. Holl, C. R. Woods, R. V. Gorbachev, Y. Cao, A. K. Geim, K. S. Novoselov, J. Burgdorfer, F. Libisch and M. Morgenstern, *Nat. Nanotechnol.*, 2018, **13**, 392–397.
21 B. Trauzettel, D. V. Bulaev, D. Loss and G. Burkard, *Nat. Phys.*, 2007, **3**, 192–196.
22 T. D. Ladd, F. Jelezko, R. Laflamme, Y. Nakamura, C. Monroe and J. L. O'Brien, *Nature*, 2010, **464**, 45–53.
23 P. Koskinen, S. Malola and H. Hakkinen, *Phys. Rev. Lett.*, 2008, **101**, 115502.
24 C. O. Girit, J. C. Meyer, R. Erni, M. D. Rossell, C. Kisielowski, L. Yang, C. H. Park, M. F. Crommie, M. L. Cohen, S. G. Louie and A. Zettl, *Science*, 2009, **323**, 1705–1708.
25 K. A. Ritter and J. W. Lyding, *Nat. Mater.*, 2009, **8**, 235–242.
26 K. Kim, S. Coh, C. Kisielowski, M. F. Crommie, S. G. Louie, M. L. Cohen and A. Zettl, *Nat. Commun.*, 2013, **4**, 2723.
27 J. Peng, W. Gao, B. K. Gupta, Z. Liu, R. Romero-Aburto, L. H. Ge, L. Song, L. B. Alemany, X. B. Zhan, G. H. Gao, S. A. Vithayathil, B. A. Kaipparettu, A. A. Marti, T. Hayashi, J. J. Zhu and P. M. Ajayan, *Nano Lett.*, 2012, **12**, 844–849.
28 M. Li, W. B. Wu, W. C. Ren, H. M. Cheng, N. J. Tang, W. Zhong and Y. W. Du, *Appl. Phys. Lett.*, 2012, **101**, 10.
29 R. Q. Ye, C. S. Xiang, J. Lin, Z. W. Peng, K. W. Huang, Z. Yan, N. P. Cook, E. L. G. Samuel, C. C. Hwang, G. D. Ruan, G. Ceriotti, A. R. O. Raji, A. A. Marti and J. M. Tour, *Nat. Commun.*, 2013, **4**, 2943.
30 Y. J. Xu, X. Y. Li, G. H. Hu, T. Wu, Y. Luo, L. Sun, T. Tang, J. F. Wen, H. Wang and M. Li, *Appl. Surf. Sci.*, 2017, **422**, 847–855.
31 Y. Luo, M. Li, L. Sun, Y. Xu, M. Li, G. Hu, T. Tang, J. Wen, X. Li, J. Zhang and L. Wang, *J. Colloid Interface Sci.*, 2018, **529**, 205–213.
32 X. L. Zhu, W. H. Wang, W. Yan, M. B. Larsen, P. Boggild, T. G. Pedersen, S. S. Xiao, J. Zi and N. A. Mortensen, *Nano Lett.*, 2014, **14**, 2907–2913.
33 Z. Liu, L. L. Ma, G. Shi, W. Zhou, Y. J. Gong, S. D. Lei, X. B. Yang, J. N. Zhang, J. J. Yu, K. P. Hackenberg, A. Babakhani, J. C. Idrobo, R. Vajtai, J. Lou and P. M. Ajayan, *Nat. Nanotechnol.*, 2013, **8**, 119–124.
34 L. Liu, J. Park, D. A. Siegel, K. F. McCarty, K. W. Clark, W. Deng, L. Basile, J. C. Idrobo, A. P. Li and G. Gu, *Science*, 2014, **343**, 163–167.
35 G. Kim, H. Lim, K. Y. Ma, A. R. Jang, G. H. Ryu, M. Jung, H. J. Shin, Z. Lee and H. S. Shin, *Nano Lett.*, 2015, **15**, 4769–4775.
36 L. X. Chen, L. He, H. S. Wang, H. M. Wang, S. J. Tang, C. X. Cong, H. Xie, L. Li, H. Xia, T. X. Li, T. R. Wu, D. L. Zhang, L. W. Deng, T. Yu, X. M. Xie and M. H. Jiang, *Nat. Commun.*, 2017, **8**, 14703.
37 D. C. Joy, *Helium Ion Microscopy Principles and Applications*, Springer, New York Heidelberg Dordrecht London, 2013.
38 G. Hlawacek, V. Veligura, R. van Gastel and B. Poelsema, *J. Vac. Sci. Technol., B*, 2014, **32**, 020801.
39 C. Casiraghi, A. Hartschuh, H. Qian, S. Piscanec, C. Georgi, A. Fasoli, K. S. Novoselov, D. M. Basko and A. C. Ferrari, *Nano Lett.*, 2009, **9**, 1433–1441.
40 L. M. Malard, M. A. Pimenta, G. Dresselhaus and M. S. Dresselhaus, *Phys. Rep.*, 2009, **473**, 51–87.
41 L. A. J. Garvie, A. J. Craven and R. Brydson, *Am. Mineral.*, 1994, **79**, 411–425.
42 K. Suenaga and M. Koshino, *Nature*, 2010, **468**, 1088–1090.
43 Z. Liu, L. H. G. Tizei, Y. Sato, Y. C. Lin, C. H. Yeh, P. W. Chiu, M. Terauchi, S. Iijima and K. Suenaga, *Small*, 2016, **12**, 252–259.
44 L. Liu, D. A. Siegel, W. Chen, P. Z. Liu, J. J. Guo, G. Duscher, C. Zhaog, H. Wang, W. L. Wang, X. D. Bai, K. F. McCarty, Z. Y. Zhang and G. Gu, *Proc. Natl. Acad. Sci. U. S. A.*, 2014, **111**, 16670–16675.
45 A. K. Geim and K. S. Novoselov, *Nat. Mater.*, 2007, **6**, 183–191.
46 L. A. Ponomarenko, F. Schedin, M. I. Katsnelson, R. Yang, E. W. Hill, K. S. Novoselov and A. K. Geim, *Science*, 2008, **320**, 356–358.
47 L. B. Tang, R. B. Ji, X. K. Cao, J. Y. Lin, H. X. Jiang, X. M. Li, K. S. Teng, C. M. Luk, S. J. Zeng, J. H. Hao and S. P. Lau, *ACS Nano*, 2012, **6**, 5102–5110.
48 S. H. Jin, D. H. Kim, G. H. Jun, S. H. Hong and S. Jeon, *ACS Nano*, 2013, **7**, 1239–1245.
49 S. J. Zhu, Y. B. Song, X. H. Zhao, J. R. Shao, J. H. Zhang and B. Yang, *Nano Res.*, 2015, **8**, 355–381.

